Published in:
Properties of silicon, R. Hull, ed.
(INSPEC, IEE, London, 1999)

Properties of rare-earth doped crystalline silicon

A. Polman
FOM-Institute for Atomic and Molecular Physics
Kruislaan 407, NL-1098 SJ Amsterdam, The Netherlands
E-mail: polman@amolf.nl, http://www.amolf.nl

S. Coffa
CNR-IMETEM
Stradale Primosole 50, I-95121 Catania, Italy
e-mail: coffa@ct.infn.it

compiled on October 15, 2003

1. Introduction

Rare earth (RE) ions, incorporated in a solid, can show sharp, atomic-like and temperature-independent optical transitions. If silicon could be effectively doped with optically active RE ions, it would be possible to achieve efficient light emission from this semiconductor, circumventing the limitations posed by its indirect band gap. This would allow combining the excellent electronic properties of Si with the attractive optical properties of rare earth ions, opening perspectives for a new class of device applications.

There are 13 luminescent RE ions: Ce, Pr, Nd, Pm, Sm, Eu, Gd, Tb, Dy, Ho, Er, Tm, and Yb. The emission wavelengths of the optical transitions in these ions range from the visible to the near infrared. When incorporated in a solid, they generally take the trivalent charge state, for which the electronic configuration is given by: $1s^2....(4f^n)5s^25p^6$, with n = 1-13, depending on the RE ion. The spin-spin and spin-orbit interactions between the $4f$ electrons define energy levels, which, because of the shielding effect of the outer closed $5s$ and $5p$ shells, are relatively sharp. The electric field induced by the near-neighbor atoms on the $4f$ electron wave functions causes a splitting of the degenerate energy levels due to the Stark effect. The number of lines by which the levels split is determined by the site symmetry. This Stark splitting, in combination with homogeneous and inhomogeneous broadening determines the energy width of optical transitions between the levels.

A schematic of the low-lying (< 1.2 eV from the ground state) $4f$ energy levels for all RE ions is given in Figure 1. The levels are indicated by the Russell-Saunders notation $^{2S+1}L_J$ with $2S+1$ the spin multiplicity, L the total orbital angular momentum, indicated by S, P, D, F,.... for L=0, 1, 2, 3, ..., and $J=L+S$ the total angular momentum. The selection rule for an electric dipole transition, $\Delta L=\pm1$, causes all optical transitions between the $4f$ levels in Figure 1 to be forbidden. However, in a solid, interactions with the outer lying wave functions or with lattice vibrations can mix other states into the $4f$ states, making the transitions possible. Due to the small spatial extent of the $4f$ wave functions, these interactions are small, and thus the oscillator strengths for intra-$4f$ transitions are small and the radiative lifetimes of the levels relatively long.

Transitions between the RE energy levels can not only occur by optical emission, but also by multiphonon relaxation. In particular for the low-energy transitions, with energy gaps of the order of typical phonon energies in the host (~ 60 meV in Si), this process will be very efficient, and the quantum efficiency for optical emission will be low. Optical transitions that may have high quantum efficiencies in Fig. 1 are e.g. those in Dy^{3+} ($^6H_{13/2}\rightarrow^6H_{15/2}$, 0.43 eV, 2.88 μm), Ho^{3+} ($^5I_7\rightarrow^5I_8$, 0.58 eV, 2.12 μm), Ho^{3+} ($^5I_6\rightarrow^5I_8$, 1.07 eV, 1.16 μm), Ho^{3+} ($^5I_6\rightarrow^5I_7$, 0.43 eV, 2.88 μm), Er^{3+} ($^4I_{13/2}\rightarrow^4I_{15/2}$, 0.81 eV, 1.53 μm), Tm^{3+} ($^3H_4\rightarrow^3H_6$, 0.67 eV, 1.86 μm), and Tm^{3+} ($^3H_5\rightarrow^3H_6$, 1.04 eV, 1.18 μm).

Rare earth doping has been widely explored for the case of insulating host such as glasses and ceramic materials. In this case, the RE ions can be optically excited, and laser emission and optical amplification can be achieved. In a semiconductor, the RE ions may also be excited electrically. One excitation mechanism is that in which an electron-hole pair (generated either optically or electrically in a *p-n* junction) can be trapped near the RE ion and then recombine while transferring its recombination energy to the RE ion in an impurity Auger process. This then brings the RE ion in an excited *4f* state. The RE ion can then decay by the emission of a photon. A schematic of this process for the case of Er in Si is given in Fig. 2(a), which shows the top of the valence (*V*) band and the bottom of the conduction (*C*) band of Si, as well as the ground ($^4I_{15/2}$) and first excited ($^4I_{13/2}$) state of Er^{3+}. The Er^{3+} energy levels are drawn below the top of the valence band as a high energy is gained by the triple ionization of Er^{3+}. The interaction between the wave functions of the three outer (valence) electrons of Er^{3+} and those of the semiconductor host results in the introduction of energy levels in the Si band gap below the bottom of the conduction band. Theoretical and experimental investigations have suggested that these levels act as pathways for the energy transfer between the electronic system of the semiconductor and the rare earth ions. The excitation of Er^{3+} then involves a two-step process: the trapping (*T*) of electrical carriers at the Er-related level in the Si band gap, and the Auger transfer excitation (*E*) of the RE ion. Note that de-trapping (*D*) and backtransfer (*B*) processes, that quench the luminescence, are also indicated. An additional quenching path may be provided by an Auger transition, in which the excited Er decays by exciting an electron in the conduction band (as shown in Fig. 2(b)) or an electron trapped at a defect level, to a higher lying state. A large amount of research is being devoted to the study of these quenching processes, and to developing ways to avoid them. Within the context of the excitation model in Fig. 2(a), only RE ions with excited states at energies lower than 1.12 eV (the Si band gap at 300 K) from the ground state can be excited. In Fig. 1, only those RE energy levels are drawn that fulfill this condition. It should be noted that the efficiency of the excitation and de-excitation processes for a specific rare-earth ion is critically dependent on the density and energy positions of the energy levels introduced in the Si band gap.

Apart from the above exciton-related excitation process, impact excitation is also possible, in which hot carriers generated in the semiconductor can excite the rare earth ions (see Fig. 2(c)). This excitation mechanism significantly differs from the previous one. First of all, no energy level in the band gap is needed to mediate the energy transfer. Secondly, there is no band gap limitation to the RE excitation, and high lying levels may be excited. In principle it would be possible to achieve visible emission as reported for Tb (green at 0.54 μm), Sm (red at 0.65 μm) and Ce (blue at 0.47 μm) in ZnS and SrS used in electroluminescent flat panel displays. However, in Si the quantum efficiency for these processes is expected to be quite low because: 1) at high electric fields impact ionization of Si (avalanche breakdown) will set in as a competitive process, and 2) the highly excited rare earth ions may efficiently de-excite though a non-radiative Auger

process by promoting an electron from the valence band to the conduction band (see Fig. 2(b)).

Most of the research on RE doped Si has focussed on erbium as an optical dopant. Erbium has a $^4I_{13/2}\rightarrow^4I_{15/2}$ intra-4f transition at a wavelength of 1.53 μm, a standard telecommunication wavelength. Research on Er-doped Si is therefore strongly motivated by the possibility to fabricate opto-electronic devices such as light emitting diodes or optical amplifiers in Si, operating at this important wavelength. Unless otherwise noted, the various properties described further on are all related to Er in Si. This article gives a concise overview of the most important materials properties known for Er in Si. The most important numbers are listed in Table I. More detailed information can be found in two Proceedings of Materials Research Society Symposia, Refs. 1 and 2.

2. Solubility, incorporation, diffusivity, reactivity

2.1 Solubility

The solubility of RE ions in pure Si is unknown. However, by analogy with the transition metals it is expected to be very low, in the 10^{14}-10^{16} cm^{-3} range. One measurement is reported[3] for the solubility of Er in CZ-Si at 1300 °C: ~10^{16} Er/cm^3. Another measurement[4] quotes an effective solubility (deduced from the onset of precipitation) of $1.3x10^{18}$ Er/cm^3. As we will discuss later on, the measured "effective" solubility is often affected by the presence of impurities, as well as by kinetic factors. In any case, such low RE concentrations are too low for any practical applications.[5] Therefore, non-equilibrium methods have to be employed in order to incorporate useful RE concentrations (10^{18}-10^{20} cm^{-3}) in Si.

2.2 Incorporation methods

Several techniques have been successfully applied to incorporate Er in crystalline Si. They are listed below, together with references to papers in which growth and synthesis parameters are specifically addressed.

- ion implantation followed by annealing [3,4,6,7,8,9,10,11,12,13,14,15]
- molecular beam epitaxy (MBE)[16,17,18,19,20,21]
- ion beam assisted sputtering (IBAS)[22]
- chemical vapor deposition (CVD)[23]
- electron-cyclotron resonance plasma enhanced ECR-CVD[24]
- evaporation followed by laser melting and diffusion.[25,26,27]

Erbium ion implantation is the most used techniques to incorporate Er in Si. When performed at low substrate temperature (80-300 K) ion implantation at fluences above ~ 4×10^{13} leads to the formation of a continuous amorphous layer. This layer can be recrystallized using thermal solid phase epitaxy (SPE) at temperatures above 500 °C. At 600 °C, the SPE rate is 0.03-0.05 nm/s, depending on the Er concentration. During SPE, segregation of Er takes place at the moving interface.[9,10] The segregation coefficient is strongly concentration dependent and ranges from 0.01 to 0.2.[14] Once a critical Er concentration at the growing interface is exceeded, the epitaxial growth breaks down and crystal twins are formed. This critical concentration decreases with growth temperature and ranges from $2x10^{20}$ Er/cm^3 at 500 °C, to $6x10^{19}$ Er/cm^3 at 900 °C. A large fraction of the incorporated concentration is believed to be in the form of Er or Er-Si precipitates. Segregation can be avoided if oxygen is co-implanted in the Er-doped region.[10,11,15]. This effect is due to the strong interaction between Er and O, which reduces the Er mobility, and enhances its solubility. Oxygen form clusters with Er, and thereby enhances the

effective solubility of Er in Si. The crystal quality of the recrystallized layer can be improved by performing ion implantation at 77 K, which results in a sharper amorphous-crystal interface and in a largely reduced density of threading dislocations.[14]

Experiments have also been performed on Pr,[10] Tb,[28] Yb,[29] and Eu[30] ion implantation into single crystal Si. A recrystallization and segregation behavior very similar to that of Er has been observed. Finally, it should be noted that amorphization can be avoided if erbium ion implantation is performed at high temperature (typically > 400 °C). This condition however leads to the formation of secondary defects (dislocations) upon annealing.[4]

MBE using separate Si and Er sources is the second most used technique. During MBE on Si(100) strong Er segregation takes place,[17,18] and a maximum concentration of $2x10^{19}$ Er/cm^3 can be incorporated in single crystal Si at a growth temperature of 600 °C. Segregation is also observed during MBE of Pr-doped Si(100).[18] When oxygen is introduced during MBE, at a partial pressure above 10^{-10} mbar, the segregation can be avoided.[17,19,21] If MBE is performed on Si(111), no Er segregation is observed,[17] and a large density of Er-Si precipitates forms,[19] which are epitaxial on Si(111).

IBAS, CVD, ECR-CVD, and laser doping are new techniques that are being explored. IBAS using an electric-mirror sputtering-type ion source has been used to fabricate well-controlled doping profiles of Er in Si, with O serving to increase the trapped Er density. Er concentrations up to $6x10^{20}$ Er/cm^3 and O concentrations up to $2x10^{20}$ O/cm^3 have been obtained.[22] In CVD processes, the main challenge is to simultaneously achieve epitaxial crystal growth and the proper decomposition of the RE precursor. Evaporation and laser melting studies are complicated by the fact that Er is highly reactive to for example oxygen.

2.3 Diffusivity

No data are available on the diffusivities of RE ions in Si, apart from one reference[3] that quotes diffusion coefficients of Er in CZ-Si: 10^{-15} cm^2/s (900 °C), and 10^{-12} cm^2/s (1300 °C), and an activation enthalpy of 4.6 eV. It should be noted that, due to the strong interaction of Er with impurities such as O and C which are intrinsic contaminants in Si, in general measurements are not representative of the true Er diffusivity in Si. Instead they represent trap-limited diffusion that is retarded or inhibited by the formation of Er-impurity complexes.

2.4 Reactivity

ErSi and $ErSi_{2-x}$ (also designated as Er_3Si_5) compounds have been reported. Er_3Si_5 was reported to be the most stable, and its (001) orientation is epitaxial on Si(111) with a mismatch of 1.2 %. The structure of ultra-thin erbium silicides on Si(111), as well as related references, are reported in Ref. 31. Er ion implantation into Czochralski grown (CZ) Si annealed at 900 °C leads to the formation of platelet shaped precipitates, attributed to $ErSi_2$, oriented along Si(111) planes. These platelets form above a critical concentration of $(1.3\pm0.4)x10^{18}$ Er/cm^3.

Erbium is extremely reactive with oxygen, and thin Er films deposited on Si will rapidly oxidize to Er_2O_3, unless extremely good vacuum conditions are held. Er_2O_3 shows clear photoluminescence at 1.55 μm, clearly distinct from the emission of Er in Si at 1.53 μm. Er also reacts very strongly with O inside Si, both in CZ-Si (that contains typically $2x10^{18}$ O/cm^3), and in O co-implanted Si.[8,32] This Er-O pairing can occur at temperatures as low at 600 °C.[32] As Er and O are so reactive, the effective solubility of Er in Si is strongly dependent on the O content and co-implantation with high O

concentrations enhances the effective solubility of Er in Si. Similar reactivity has been observed also for and F co-implantation.

3. Site structure

Theoretical calculations have shown that the lowest energy configuration of isolated Er in Si is a tetrahedral interstitial site.[33] Experimentally, Er is mostly observed in the form of Er-Si precipitates or in complexes with intentionally added impurities such as for example O. In Er-implanted float-zone grown (FZ) Si (with very low O content), annealed at 900 °C, Er is coordinated with twelve Si atoms at a mean distance of 3.00 Å, similar to the Er-Si bond length in $ErSi_2$. In contrast, in CZ-Si Er is coordinated with roughly 6 O atoms at a mean distance of 2.25±0.03 Å, similar to the Er-O distance in Er_2O_3. A similar O-rich environment has also been found in Er and O coimplanted samples[32] where an oxygen cage around Er is already observed after recrystallization of the amorphous layer at 620 °C.

Attempts have been made to study the site symmetry of Er in Si by high-resolution photoluminescence spectroscopy. As the luminescence spectrum is critically dependent on small changes in the preparation and annealing conditions,[34] as well as on the amount of impurity co-doping, it seems difficult to make general statements on the site of Er in Si. However, cubic centers, assigned as isolated interstitial Er, have been reported in FZ-Si.[35,36] In CZ-Si a relatively small density of such sites are also found, but the dominant sites have a symmetry close to axial. Electron paramagnetic resonance experiments[37] on Er and O implanted Si gave indications of Er located in a distorted tetrahedrally coordinated Er-O complex.

4. Electrical properties

Both in FZ-Si and CZ-Si, erbium introduces a wide range of defect levels in the Si band gap, with energies ranging from 40 to 500 meV below the conduction band.[38,39,40,41] Most of these levels act as donors, so that the concentration of free electrons increases with Er concentration. The maximum free electron concentration is $6x10^{15}$ cm^{-3} in FZ-Si, and 2-$5x10^{16}$ cm^{-3} in CZ-Si. In CZ-Si, for Er concentrations below < $5x10^{17}$ cm^{-3}, the maximum electrical activity is 10 % (at 300 K). The difference between FZ-Si and CZ-Si is attributed to the different O concentration in these materials. Indeed, co-implantation of additional O (or F) can further increase the donor concentration. When hot implants are used, the relative number of O atoms required to obtain an electrically active Er ion increases logarithmically with Er dose, which is attributed to increased O and Er precipitation and extended defect formation at high implantation fluences. The highest electrical activity is obtained after annealing of low-temperature implants that result in the initial formation of a continuous amorphous layer. For example, for an Er:O ratio=1:10 and an Er concentration between $5x10^{17}$ cm^{-3}-$5x10^{19}$ cm^{-3} the donor efficiency can be as high as 80-100 %.[15,39,40]

Co-doping with impurities such as O and F causes a significant change in the deep level spectrum.[39,40,41] In pure epitaxial Si, Er-defect complexes introduce deep levels below the Si conduction band (E_C) at E_C-0.2 eV, E_C-0.26 eV, E_C-0.33 eV, E_C-0.51 eV. When impurities are present the density of deep traps is reduced and more shallow levels at E_C-0.16 eV, E_C-0.11 eV, E_C-0.08 eV are observed. This effect results in an increased Er excitation rate, and increases the effective minority carrier lifetime. These two effects increase the quantum efficiency of the Er excitation process and reduce the temperature quenching of the luminescence. Measurements of the minority carrier lifetime of Er-

doped Si have been made and are in the 1-2 μs range. when proper co-doping with O is performed.

5. Optical properties

Photoluminescence (PL) spectroscopy using optical pumping in the Si conduction band is mostly used to characterize Er-doped Si. In this case the Er is excited by photogenerated carriers that have thermalized to the bottom of the conduction band. The Er luminescence spectrum peaks around 1.53 μm. At low temperature, it shows a multiply-peaked structure with the number of lines and their relative intensity being determined by the preparation conditions (implantation parameters, MBE growth temperature, thermal annealing temperature, Er concentration, and impurity co-doping). While the number of lines in principle reflects the Er site symmetry in the crystalline host, in most cases (but not all) such symmetry information can not be deduced due to the broad distribution of sites with each a different geometry. At high temperatures, the Er PL spectrum broadens due to the excitation of hot lines in the various manifolds, and due to homogeneous broadening.

In the standard PL configuration, with above-band gap excitation, the Er luminescence intensity is determined by three factors:

1) the concentration of optically active Er sites, that is thought to depend on the impurity co-doping level, as impurities enhance the effective solubility of Er,[7,42] Ion implantation experiments[43] at a fixed energy but varying ion fluence have shown that the PL intensity in CZ-Si saturates above a Er concentration of $3x10^{17}$ Er/cm^3. In IBAS experiments, a maximum PL intensity was obtained for an Er concentration of $2x10^{18}$ Er/cm^3. This limit was the same for pure and O co-doped Si, although the intensity for O co-doped material was more than 10 times higher. In MBE experiments, optimum PL intensity was obtained using a background pressure of 10^{-10}–10^{-9} mbar.[44]

2) the Er excitation efficiency, which depends on the structure of the Er-impurity complex. At high temperature the effective excitation rate is reduced due to dissociation of trapped carriers or excitons (step D in Fig. 2(a)), and therefore it depends strongly on the depth of the Er-related level below the conduction band. The excitation rate is also critically dependent on the minority carrier lifetime, which in turn depends on the impurity co-doping levels. In ion implanted samples, ion damage left after annealing, may dominate the carrier lifetime. In Er-implanted CZ-Si the minority carrier lifetime did not depend on Er concentration, indicating that the Er itself is not the dominant carrier trap in CZ-Si. At high temperature the excitation efficiency is also reduced in samples that show enhanced surface recombination.[45]

3) the Er luminescence quantum efficiency.

Once the Er is excited, the luminescence can be quenched by non-radiative processes such as e.g. a backtransfer process (step B in Fig. 2(a)), coupling to defect states, or due to Auger quenching (Fig. 2(b)) to free carriers.[46,47,54] Such non-radiative processes lead to a reduction in the Er luminescence lifetime at high temperature as is indeed observed.[48,49] Typical 1.53 μm Er luminescence lifetimes in crystal Si range from 1-2 ms at 10 K to < 1 μs above 200 K. In addition, a reduction in the excitation efficiency at high temperatures is also observed.

An overall internal quantum efficiency (including excitation and luminescence efficiency) as high as 10% can be achieved at 15 K at low pump power.[50,54] At higher temperature or higher pump power the quantum efficiency is strongly reduced due to a reduction in luminescence quantum efficiency (due to Auger quenching and/or backtransfer) and in excitation efficiency (due to de-trapping).

In summary, optimization of the Er luminescence involves the simultaneous consideration of a large number of related parameters that all affect the Er active fraction, excitation efficiency, and luminescence quantum efficiency in a different way.

6. Applications and device prospects

Erbium-doped crystalline Si light emitting diodes (LED's) have been fabricated that show 1.53 μm emission at 77 K,[51] and at 300 K.[19,52,53,54] Electroluminescence was obtained both in forward bias due to carrier recombination trapping excitation and in reverse bias due to impact excitation. In the latter case the Er luminescence spectrum is superimposed on a broad background ranging from the visible into the near infrared, due to hot carrier luminescence. The excitation cross sections for electron-hole mediated and impact excitation were determined to be $4x10^{-15}$ cm^2 and > $6x10^{-17}$ cm^2, respectively. In spite of the lower excitation cross section, room temperature electroluminescence in reverse bias is a factor of ~20 higher than in forward bias.[55] This is due to: a) the reduced temperature quenching (a factor 3 in reverse bias, compared to a factor 30 in forward bias, between 77 and 300 K); and b) inhibition of the strong Auger de-excitation in the depletion layer of a p-n junction if Er is excited by impact excitation. Under reverse bias typical quantum efficiencies at room temperature were in the 10^{-3}-10^{-4} range. Quite interestingly, it was found that these LED's have a faster switching time than would be expected on the basis of the measured Er luminescence lifetime, since at the diode turn-off Er ions are rapidly quenched by Auger quenching in the heavily doped neutral region of the diode.[46,55] Modulation at frequencies of 10-50 MHz can be achieved.

References

[1] *Rare earth doped semiconductors*, Mater. Res. Soc. Proc. **301** (1993), edited by G.S. Pomrenke, P.B. Klein, and D.W. Langer.
[2] *Rare earth doped semiconductors II*, Mater. Res. Soc. Proc. **422** (1996), edited by S. Coffa, A. Polman, and R.N. Schwartz.
[3] F.Y.G. Ren, J. Michel, Q. Sun-Paduano, B. Zheng, H. Kitagawa, D.C. Jacobson, J.M. Poate, and L.C. Kimerling, Ref. 2, p. 87.
[4] D.J. Eaglesham, J. Michel, E.A. Fitzgerald, D.C. Jacobson, J.M. Poate, J.L. Benton, A. Polman, Y.-H. Xie, and L.C. Kimerling, Appl. Phys. Lett. **58**, 2797 (1991).
[5] Y.H. Xie, E.A. Fitzgerald, and Y.J. Mii, J. Appl. Phys. **70**, 3233 (1991).
[6] H. Ennen, J. Schneider, G. Pomrenke, and A. Axmann, Appl. Phys. Lett. **43**, 943 (1983).
[7] J. Michel, J.L. Benton, R.F. Ferrante, D.C. Jacobson, D.J. Eaglesham, E.A. Fitzgerald, Y.-H. Xie, J.M. Poate, and L.C. Kimerling, J. Appl. Phys. **70**, 2667 (1991).
[8] D.L. Adler, D.C. Jacobson, D.J. Eaglesham, M.A. Marcus, J.L. Benton, J.M. Poate, and P.H. Citrin, Appl. Phys. Lett. **61**, 2181 (1992).
[9] A. Polman, J.S. Custer, E. Snoeks, and G.N. van den Hoven, Appl. Phys. Lett. **62**, 507 (1993).
[10] J.S. Custer, A. Polman, and M.H. van Pinxteren, J. Appl. Phys. **75**, 2809 (1994).
[11] S. Coffa, F. Priolo, G. Franzò, V. Bellani, A. Carnera, and C. Spinella, Phys. Rev. B **48**, 11782 (1993).
[12] J. Michel, F.Y.G. Ren, B. Zheng, D.C. Jacobson, J.M. Poate, and L.C. Kimerling, Mat. Sci. Forum **143-147**, 707 (1994).
[13] P. Liu, J.P. Zhang, R.J. Wilson, G. Curello, and S.S. Rao, Appl. Phys. Lett. **66**, 3158 (1995).
[14] A. Polman, J.S. Custer, P.M. Zagwijn, A.M. Molenbroek, and P.F.A. Alkemade, J. Appl. Phys. **81**, 150 (1997).
[15] F. Priolo, S. Coffa, G. Franzò, C. Spinella, A. Carnera, and V. Bellani, J. Appl. Phys. **74**, 4936 (1993).
[16] H. Ennen, G. Pomrenke, A. Axmann, K. Eisele, W. Haydl, and J. Schneider, Appl. Phys. Lett. **46**, 381 (1985).
[17] R. Serna, M. Lohmeier, P.M. Zagwijn, E. Vlieg, and A. Polman, Appl. Phys. Lett. **66**, 1385 (1995).
[18] K. Miyashita, Y. Shiraki, D.C. Houghton, and S. Fukatsu, Appl. Phys. Lett. **67**, 235 (1995).

[19] J. Stimmer, A. Reittinger, J.F. Nützel, G. Abstreiter, H. Holzbrecher, and Ch. Buchal, Appl. Phys. Lett. **68**, 3290 (1996).
[20] A. Polman, R. Serna, J.S. Custer, and M. Lohmeier, Mat. Res. Soc. Proc. **422**, 21 (1996).
[21] J. Stimmer, A. Reittinger, G. Abstreiter, H. Holzbrecher, and Ch. Buchal, Ref. 2, p. 15.
[22] M. Matsuoka, and Shun-ichi Tohno, J. Appl. Phys. **78**, 2751 (1995).
[23] M. Morse, B. Zheng, J. Palm, X. Duan, and L.C. Kimerling, Ref. 2, p. 41.
[24] P.S. Andry, W.J. Varhue, E. Adams, M. Lavoie, P.B. Klein, R. Hengehold, and J. Hunter, Ref. 2, p.57.
[25] K. Nakashima, Ref. 1, p. 61.
[26] T. Asatsuma, P. Dodd, J.F. Donegan, J.G. Lunney, and J. Hegarty, Ref. 1, p. 67.
[27] K. Nakashima, O. Eryu, O. Iioka, H. Minami, and M. Watanabe, Ref. 2, p. 75.
[28] G.N. van den Hoven, A. Polman, S. Coffa, and F. Priolo, unpublished.
[29] T. Xu, P. Zhu, D. Li, T. Ren, H. Sun, and S. Wan, Physics Lett. A **189**, 423 (1994).
[30] A. Bhagawat, M.P. Kurup, K.G. Prasad, and R.P. Sharma, Nucl. Instr. Meth. Res. B **33**, 719 (1988).
[31] M. Lohmeier, W.J. Huisman, G. ter Horst, P.M. Zagwijn, A. Nishiyama, C.L. Nicklin, T.S. Turner, and E. Vlieg, Mater. Res. Soc. Proc. **355**, 281 (1995).
[32] A. Terrasi, G. Franzò, S, Coffa, F. Priolo, D. D'Acapito and S. Mobilio, Appl. Phys. Lett. **70**, 1712 (1997)
[33] M. Needles, M. Schlüter, and M. Lannoo, Phys. Rev. B. **47**, 15533 (1993).
[34] J.H. Shin and A. Polman, unpublished.
[35] H. Przybylinska, G. Hendorfer, M. Bruckner, L. Palmetshofer, and W. Jantsch, Appl. Phys. Lett. **66**, 490 (1995).
[36] H. Przybylinska, W. Jantsch, Y. Suprun-Belevitch, M. Stepikhova, L. Palmetshofer, G. Hendorfer, A. Kozanecki, R.J. Wilson, and B.J. Sealy, Phys. Rev. B **54**, 2532 (1996).
[37] J.D. Carey, J.F. Donegan, R.C. Barklie, F. Priolo, G. Franzò, and S. Coffa, Appl. Phys. Lett. **69**, 3854 (1996).
[38] J.L. Benton, J. Michel, L.C. Kimerling, D.C. Jacobson, Y.-H. Xie, D.J. Eaglesham, E.A. Fitzgerald, and J.M. Poate, J. Appl. Phys. **70**, 2667 (1991).
[39] F. Priolo, G. Franzò, S. Coffa, A. Polman, S. Libertino, R. Barklie, and D. Carey, J. Appl. Phys. **78**, 3874 (1995).
[40] S. Libertino, S. Coffa, G. Franzò, and F. Priolo, J. Appl. Phys. **78**, 3867 (1995).
[41] S. Libertino, S. Coffa, R. Mosca, and E. Gombia, Ref. 2, p. 113.
[42] P. Liu, J.P. Zhang, R.J. Wilson, G. Curello, S.S. Rao, and P.L.F. Hemment, Appl. Phys. Lett. **66**, 3158 (1995).
[43] A. Polman, G.N. van den Hoven, J.S. Custer, J.H. Shin, and R. Serna, J. Appl. Phys. **77**, 1256 (1995).
[44] J. Stimmer, A. Reittinger, G. Abstreiter, H. Holzbrecher, and Ch. Buchal, Ref. 2, p. 15.
[45] J. Michel, F.Y.G. Ren, B. Zheng, D.C. Jacobson, J.M. Poate, and L.C. Kimerling, Mat. Sci. Forum **143-147**, 707 (1994).
[46] S. Coffa, G. Franzò, and F. Priolo, Appl. Phys. Lett. **69**, 2077 (1996).
[47] T. Gregorkiewicz, I. Tsimperides, C.A.J. Ammerlaan, F.P. Widdershoven, and N.A. Sobolev, Ref. 2, p. 207.
[48] S. Coffa, F. Franzò, F. Priolo, A. Polman, and R. Serna, Phys. Rev. B **49**, 16313 (1994).
[49] P.G. Kik, K. Kikoin, and A. Polman, Appl. Phys. Lett. **70**, 1721 (1997).
[50] G. Franzò, S. Coffa, F. Priolo, submitted to Phys. Rev. B.
[51] H. Ennen, G. Pomrenke, A. Axmann, K. Eisele, W. Haydl, and J. Schneider, Appl. Phys. Lett **46**, 381 (1985).
[52] G. Franzò, F. Priolo, S. Coffa, A. Polman, and A. Carnera, Appl. Phys. Lett. **64**, 2235 (1994).
[53] B. Zheng, J. Michel, F.Y.G. Ren, L.C. Kimerling, D.C. Jacobson, and J.M. Poate, Appl. Phys. Lett. **64**, 2842 (1994).
[54] J. Palm, F. Gan, B. Zheng, J. Michel, and L.C. Kimerling, Phys. Rev. B **54**, 17603 (1996).
[55] G. Franzò, S. Coffa, F. Priolo, and C. Spinella, J. Appl. Phys. **81**, 2784 (1997).

TABLE I Review of properties of erbium-doped crystalline silicon

PARAMETER	**VALUE**	**REF.**	**COMMENTS**
solubility in CZ-Si	$2x10^{16}$ cm^{-3}	3	at 1300 °C
effective solubility in CZ-Si	$1.3x10^{18}$ cm^{-3}	4	at 900 °C
SPE rate of Er-doped a-Si on c-Si	0.03-0.05 nm/s	10	at 600 °C, depending on [Er]
segregation coefficient during SPE	0.01-0.2	14	depending on [Er]
maximum Er concentration trapped in single crystal Si	$2x10^{20}$ cm^{-3} $2x10^{19}$ cm^{-3}	10 17	SPE at 500 °C, MBE at 600 °C
maximum Er concentration in crystal Si:O	$1x10^{19}$ cm^{-3} $>4x10^{19}$ cm^{-3} $6x10^{20}$ cm^{-3}	11 19 22	SPE at 620 °C, 10^{20} O/cm^3 MBE at 500 °C, $>8x10^{20}$ O/cm^3 IBAS at 500 °C, $2x10^{20}$ O/cm^3
diffusivity in c-Si	10^{-15} cm^2/s 10^{-12} cm^2/s	3	at 900 °C at 1300 °C
Er coordination number, bond length	12, 3.00 Å 6, 2.25 Å	8 8	FZ-Si, first shell = Si CZ-Si, first shell = O
Er electrical activation	10 % 80-100 %	38 15,39, 40	CZ-Si,300 K, [Er]<$5x10^{17}$ cm^{-3} Si:O at 300 K, for Er:O ratio = 1:10 and [Er] < $5x10^{19}$ cm^{-3}
Er donor levels in epi-Si (from E_C)	0.51, 0.33, 0.26, 0.2 eV 0.16, 0.11, 0.08 eV	40, 41	Er in epi-Si Er+O in epi-Si
minority carrier lifetime	0.69 1.7 μs	41	Er implanted epi Si Er+O implanted Si
Er^{3+} $^4I_{13/2} \rightarrow {}^4I_{15/2}$ transition peak emission wavelength	1.53-1.54 μm	1,2	at 12-300 K, with and without co-doping
electroluminescence excitation cross section	$> 4x10^{-15}$ cm^2 $> 6x10^{-17}$ cm^2	55 55	300 K, forward bias 300 K, reverse bias impact excitation

Table I Overview of known properties of erbium doped crystalline silicon

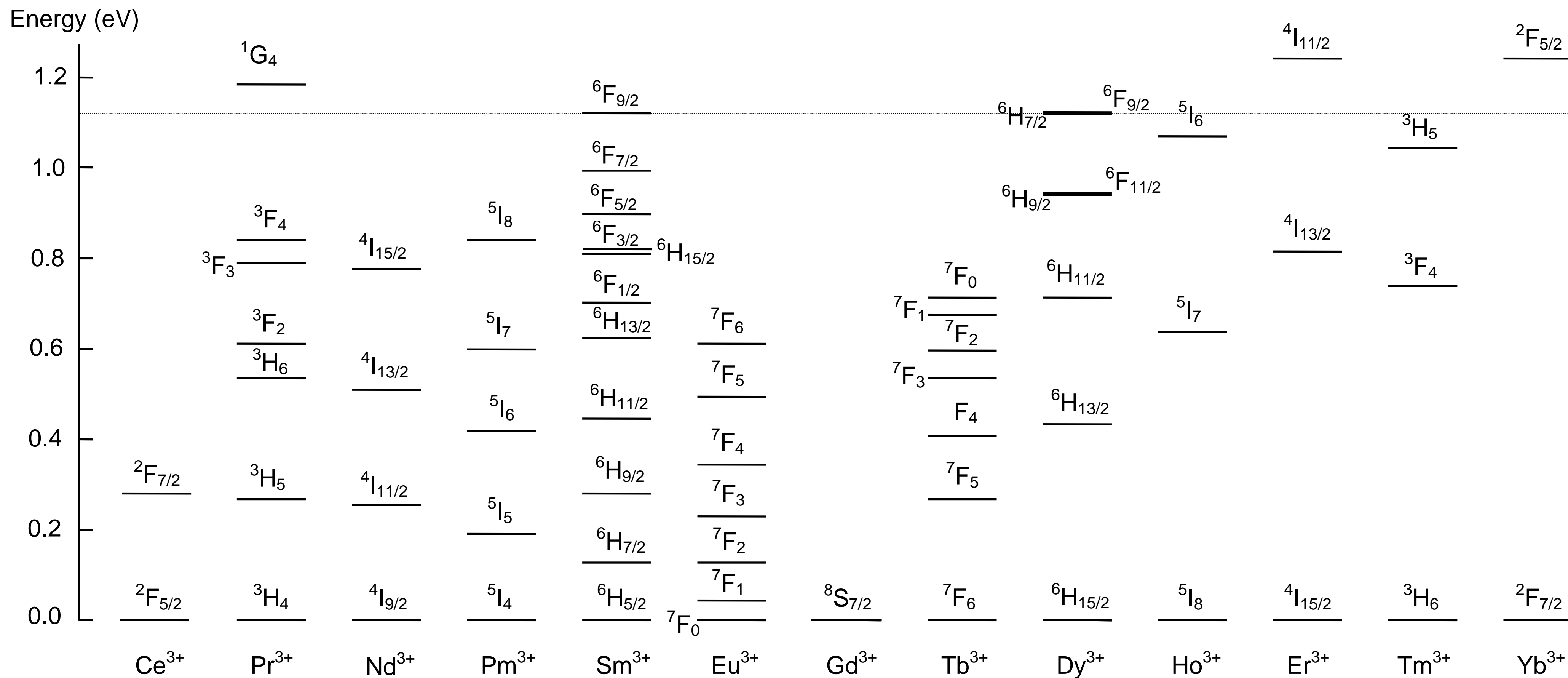

Figure 1 Schematic of energy levels of luminescent rare earth ions. Only those levels are indicated that are less than 1.2 eV from the ground state. The Si bandgap at 300 K (1.12 eV) is indicated by the dashed line. (Adapted from S. Hüfner, *Optical Spectra of Transparent Rare Earth Compounds*, (Academic, New York, 1978))

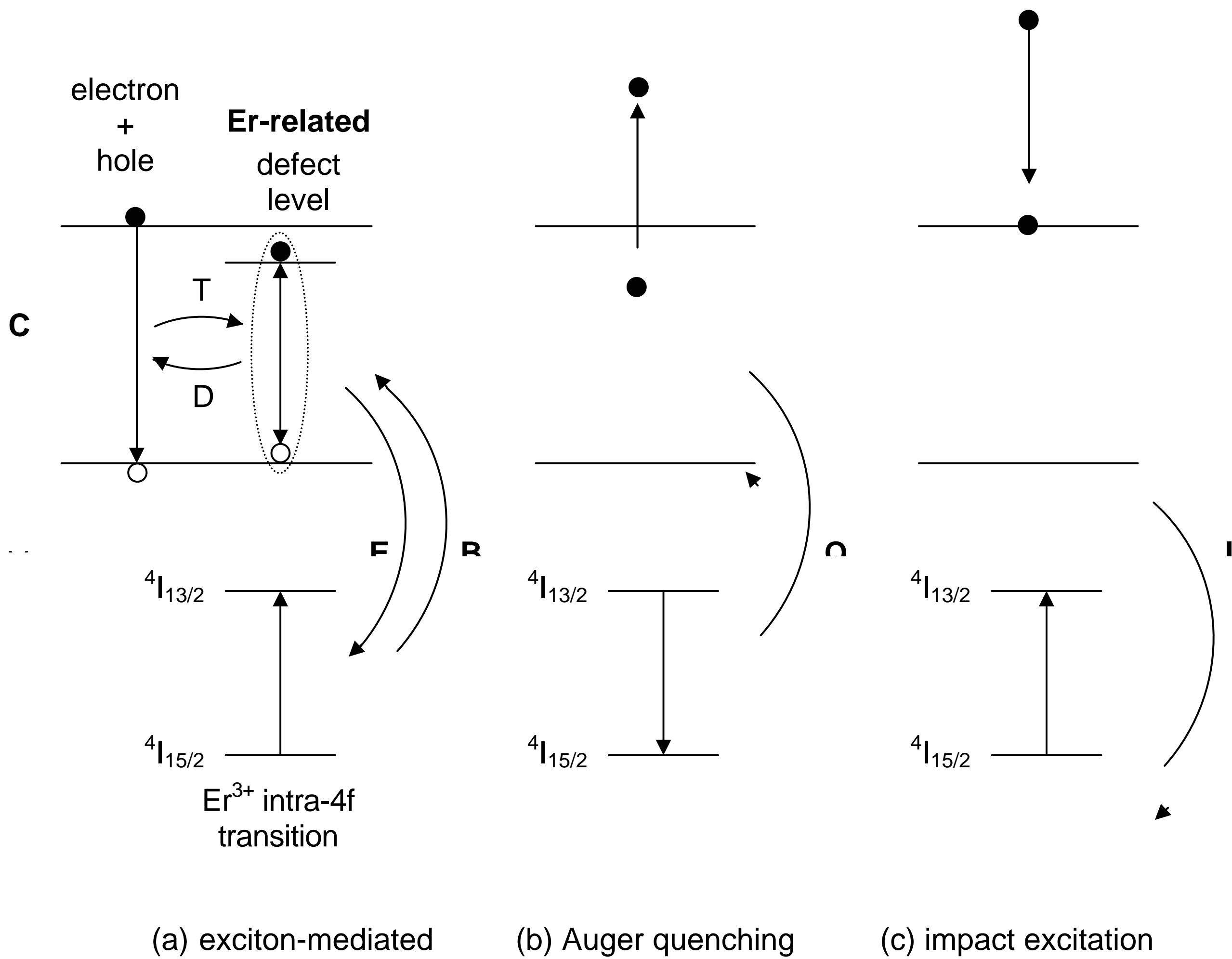

Figure 2 Schematic diagram of the electrical excitation of Er in Si. (a) Exciton-mediated excitation and deexcitation. The top of the Si valence band (*V*) and the bottom of the Si conduction band (*C*) are indicated, as well as the $^4I_{13/2}$ and $^4I_{15/2}$ first excited and ground states of Er^{3+}. Energy transfer processes are indicated: trapping (*T*), excitation (*E*), de-trapping (*D*), and backtransfer (*B*), (b) Auger quenching (*Q*) of excited Er^{3+} to free carriers, (c) Impact excitation (*I*) of Er^{3+} by hot carriers.